ELECTRICAL BEHAVIOUR AND TRANSPORT PROPERTIES IN CARBONATE SEDIMENTARY CORES

A. CEREPI

Institut EGID-Bordeaux 3, Université Michel de Montaigne Bordeaux 3, 1, allée Daguin, 33 607, Pessac, cedex, France, Tel. : 33 (05) 57 12 10 01; Fax : 33 (05) 57 12 10 11

This paper was prepared for presentation at the International Symposium of the Society of Core Analysts held in Abu Dhabi, UAE, 5-9 October, 2004.

Abstract

The paper reports an investigation of porous solid structure effects on their electrical behaviour at different frequencies and different saturations and gives the permeability prediction from the electrical behaviour of carbonate sedimentary porous systems. The electrical behaviour of porous solids is obtained from a special new configuration of loan Mk2 "LLC" Modular Universal Stackable P_c&I_R system developed to obtain different electrical measurements and capillary pressure curves. The saturation exponent n depends strongly on the frequency and ranges between 1.2 and 3.4. A non-linear behaviour is observed. This is due to the high microporosity development and its roughness. The highest value of *n* is obtained for karstic dolomite textures. The frequency dispersion is explained by the chargeability factor which depends strongly on the sedimentary rock texture and the brine/gas saturation.

INTRODUCTION

The electrical properties of sedimentary porous solids play an important role in geology, geophysics and reservoir engineering. Investigating transport properties in porous media such as electrical conductivity and permeability has many important applications in various fields such as the oil and gas production and the disposal of hazardous wastes and groundwater flow. We report an investigation of the porous solid structure effects on their electrical behaviour at different frequencies and different saturations. Then, by using different models we obtain the permeability prediction from the electrical behaviour and structure parameters. The electrical conductivity of a porous solid depends on different parameters such as the spatial distribution of the constituent minerals and pore space, the saturation distribution, the mineralogical content, wettability and temperature, with the pore structure playing the dominant role. The electrical behaviour of porous solids can be explained by different parameters such as the formation resistivity factor, the cementation factor, the resistivity index and the saturation exponent. Different studies have shown that

the complex electrical behaviour of a porous solid submitted to an alternative electrical field can be used to estimate rock petrophysical properties such as the specific surface area and permeability. The permeability is linked to different properties of the pore space, such as porosity and several structural parameters. Different empirical approaches were used to describe the observed highly non-linear dependence of permeability on porosity by exponential or power-law relationships.

THEORETICAL BACKGROUND

In isotropic homogeneous saturated porous media the electrical conductivity and porosity are related by Archie's relationship as following [1-2]:

$$F \equiv \lim_{\sigma s \to 0} \left(\frac{\sigma w}{\sigma} \right) \equiv a \Phi^{-m} \tag{1}$$

where σ is the macroscopic electrical conductivity, σ_w is the pore fluid conductivity and σ_s represents surface conductivity. Here a is a factor depending on lithology and m is the cementation factor which depends on rock structure. The parameters a and m vary in the range of $0.6 < a < 2$ and $1 < m < 3$ [3, 4]. The higher the formation factor is, the less well connected the pore space becomes. When the water saturation S_w of a porous rock decreases, due to the hydrocarbures invasion, the resistivity R_t increases. In non saturated cores, Archie found the following relationship:

$$I_R = \frac{R_t}{R_o} = S_w^{-n} \tag{2}$$

where R_o is the saturated core resistivity for $S_w = 1$; R_t is core resistivity for $S_w \leq 1$; I_R is the resistivity index and n is the saturation exponent.

The complex electrical behaviour of porous solids can be characterized by the dependence of the complex resistivity and conductivity on frequency as well as the water content, the pore microgeometry, the pressure and the temperature [5, 6]. The complex conductivity σ can be expressed

by the following relationship :

$$\sigma = YL / A = \sigma' + j\sigma'' \quad (3)$$

where σ' and σ″ are the real and imaginary conductivies; Y is admittance; L is its length; A is the cross-sectional area of the sample. Seigel [7] introduced the "chargeability" concept linked to the variation of the observed voltage in time-domain measurements. The empirical parameter of the chargeability factor (*M*) explained the frequency dispersion and is defined as follows [7-8]:

$$M = \frac{\sigma_{\omega\to\infty} - \sigma_{\omega\to 0}}{\sigma_{\omega\to\infty}} \quad (4)$$

This parameter is dimensionless and is defined in the interval $0 \le M < 1$. It corresponds to the maximum dispersion in the amplitude of σ as a varying function of frequency, normalized to its maximum value at high frequencies. When using the limit values obtained from equation (4), these parameters become:

$$M = \frac{R}{R + R_s} \quad (5)$$

PERMEABILITY PREDICTION FROM ELECTRICAL BEHAVIOUR

Permeability prediction from electrical Archie's model

Worthington [5] gives a synthesized study of different parts of Archie's law related to permeability prediction keys from the electrical behaviour and structural parameters of a porous medium. Archie [1] also presented an analogous relationship between intergranular permeability k and the formation factor F:

$$k = (b/F)^{1/c} \quad (6)$$

where b and c are empirical constants. This equation shows a linear negative gradient when plotted bilogarithmically. It was established using core data and could be applied only to resistivity logs run in water zones. When applied to groundwater problems equation (6) is also affected by departures from the Archie conditions governing the formation water salinity. In this case the equation shows positive linear gradients on a bilogarithmic plot as salinity is reduced further into fresh water. It then takes the form:

$$k = g / F_a^{\,h} \quad (7)$$

where g and h are empirical constants established from core analyses or directly from field data.

Permeability prediction from electrical Katz & Thompson's model

Katz and Thompson's model [9-10] interprets transport properties within pore solids in terms of percolation ideas. From that, they introduced a fractal percolation model to predict the permeability of disordered porous media. They recognized that mercury injection defines the first connected path and, hence, the diameter of the smallest pores on that path. So, the permeability of rocks saturated with a single liquid phase is given from the following relationship:

$$k_{KT} = Cl_c^2\left(\frac{\sigma_o}{\sigma_w}\right) = Cl_c^2\frac{1}{F} = Cl_c^2\frac{R_w}{R_o}\frac{A}{L} \tag{8}$$

where the permeability k_{KT} is defined by the Darcy relation; C is a constant on the order of 1/226. Here l_c is some characteristic length of the pore space which sets the scale for the permeability.

Permeability prediction from electrical JPK model

Several authors [11-12] have studied the effects of surface conductivity, microstructure and diffusion processes on the porous media thoroughly in the DC-frequency limit. In the JPK model, the surface conduction is accounted through the specific surface conductance and the length scale Λ_e can be interpreted as an effective pore radius for transport in the interconnected pore space volume. The length scale is related to the formation factor F and to Archie's exponent m by the relationship [11]:

$$\frac{2}{\Lambda_e} = \frac{d\log F}{d\log\Phi}\cdot\frac{S_o}{\Phi} \equiv -m\cdot\frac{S_o}{\Phi} \tag{9}$$

where S_o is the specific surface area. Some authors such as Schwartz et al. [13] and Johnson and Sen [14] proposed in the case of granular material with spherical grains another relationship for the permeability:

$$k_{JSC} = \frac{\Lambda_e^2}{8F} = \frac{\Phi^2}{32\cdot F\cdot m^2\cdot S_o^2} \tag{10}$$

EXPERIMENTAL SETTING

A special new configuration of loan Mk2 "LLC" Modular Universal Stackable $P_c\&I_R$ system is developed to obtain different electrical measurements and capillary pressure curves (Figure 1 I). The apparatus contains multi-potential electrodes along the sample length which allow us to identify the electrical behavior heterogeneity of each sample.

The sample plugs are 3.8 mm in diameter varying in length from 3 to 8 cm. The electrical cell is connected with an impedencemeter HP which allows us to make different frequencies for resistivity measurements from 100 Hz to 100 kHz for a voltage of 1000 mV. Two kinds of electrical resistivity measurements can be made: the two-electrode method using only two electrodes and the four-electrode method using two additional electrodes. In the four-electrode method, the two end metal plates serve as current electrodes and two additional electrodes around the samples measure the voltage (Figure 1 I). The volume of the sample whose resistivity is measured is situated between the two additional voltage electrodes. In order to study the frequency dependence of partially saturated rocks, the desaturation technique using semi-permeable capillary diaphragms (ceramic membranes) has been used. The brine used for all the I_R experiments was 5 g/l NaCl. The main advantages of this method are the reduction of capillary end effects and the uniform saturation distribution along the core length. In the two-electrode method, the volume of the sample whose resistivity is calculated, is situated between two current metal discs. In this case, we can observe an abnormally high resistance, the so-called contact resistance, between metal discs as current electrodes and the ends of the sample. Core plugs were drilled in parallel with the orientation of the stratification. Then, the samples were oven dried for 48 hours at a temperature of 50 °C. The dried samples were then saturated with brine under 0.001 mbar vacuum for 24 hours. We gradually increased the capillary pressure to reach the atmospheric pressure. Then, the effective water porosity was obtained by weighing. Once the sample is saturated at 100%, we assemble it with the jacket and the electrode pins into the pressure tube (confining pressure 29,5 bar max). Resistivities were measured at different saturations and different frequencies.

The water permeability k_w is obtained from the pressure drop ΔP versus Darcy velocity V_f curves for different limestone samples. The volume flow rate Q_f is set by the syringe pump, and the Darcy velocity V_f is found from the ratio Q_f / A where A is the cross-sectional area. The pressure drop is measured and divided by the sample length l. The permeability is given by the ratio η / m, where m is the slope of the line fitted to the data and η is the water viscosity.

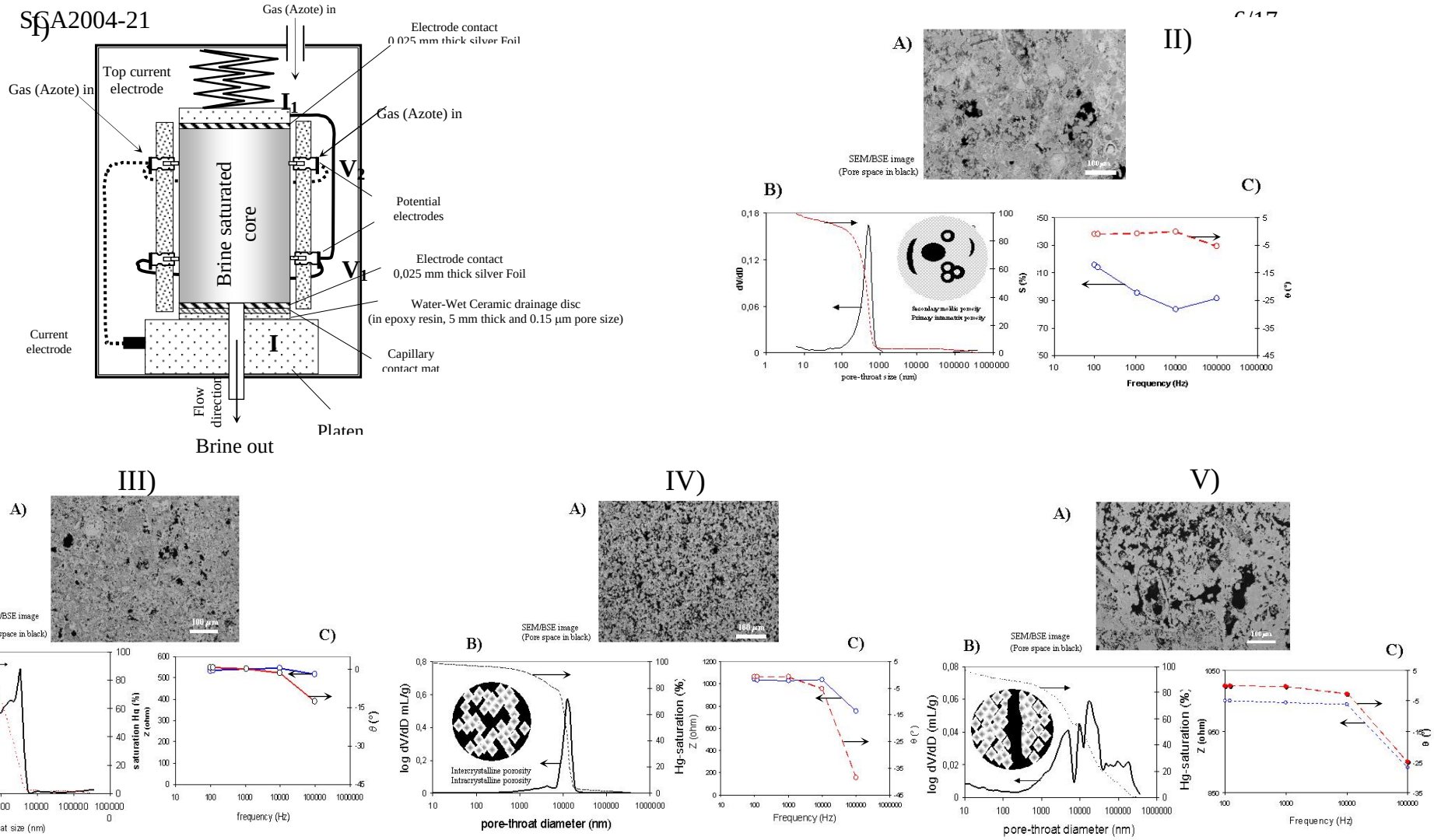

Figure 1. I) Multi - electrode core flow cell configuration for I_R-n and F-m determination; II) A) SEM/BSE image of the texture I (mudstone-wackestone-packstone) with intramatrix and intragranular porosity (sample 9-SC2). B) Hg-injection curve and pore structure. C) Electrical behaviour in different frequencies; III) A) SEM/BSE image of the texture II with intergranular and intragranular porosity (sample 7-SC3). B) Hg-injection curve and pore structure. C) Electrical behaviour in different frequencies. IV) A) SEM/BSE image of the texture III with intercrystalline porosity, intergranular and intramatrix porosity (sample 2-C). B) Hg-injection curve and pore structure. C) Electrical behaviour in different frequencies; V) A) SEM/BSE image of the texture IV (crystal carbonate) with intercrystalline porosity, intracrystalline porosity, vuggy porosity and karst (sample 9-D). B) Hg-injection curve and pore structure. C) Electrical behaviour in different frequencies;

Pore structure measurements by Hg-injection

The Hg-injection is used to obtain the pore-throat size by the relationship [15-16]:

$$P_c = 2\gamma|\cos\theta|/R_c \quad (11)$$

where P_c is the capillary pressure; R_c is the average pore-throat size (μm); θ is the angle between mercury menisc and pore wall (for mercury θ=140°); γ is the interfacial tension (for mercury γ = 0.480 N/m). Hg-injection curves give us the pore structure measurements such as mercury porosity, the distribution of the Hg-saturation versus the pore-throat size; the specific surface area. Hg-injection allows us to obtain also the characteristic length l_c defined as the smallest pores size in the connected path of the largest pores following the relationship.

TEXTURE AND PORE-TYPES IN THE STUDIED SAMPLES

Different studied samples coming from the Danian dolomite and Oligocene carbonate rocks in the Aquitain Basin have been chosen for this study because of their high textural heterogeneity due to variable depositional environments and different diagenetic evolutions (Table 1). Detailed petrographic analyses of the porous microstructures were made from thin-sections in conventional optical microscopy and Scanning Electron Microscopy (SEM), resulting in the six main defined rock-textures e.g., (Table 1, Figure 1). *Texture I* (mudstone-wackestone-packstone with mud-supported texture and with grain-supported texture) is characterised by primary pore-types: intramatrix (within carbonate mud) and intragranular pores of small size (<1-2 μm) (within carbonate grains). Their pore networks are monomodal, with low porosity-low permeability trends. *Texture II* is a mudstone-dolomitic rock-type characterized by the dominance of well-developed dolomite crystals. Pore-types were mainly intercrystalline and intracrystalline porosity. The pore structure is monomodal. *Texture III* (crystal carbonate) is a secondary dolomitic texture characterized by the dominance of the vuggy porosity, the intercrystalline porosity and the intracrystalline porosity. The pore structure is monomodal. *Texture IV* (crystal carbonate) is a secondary dolomitic texture characterized by the dominance of the most common porosity types in the dolomitized parts: vuggy porosity, intercrystalline porosity, intracrystalline porosity, karst and fracture porosity. The pore structures vary from monomodal to tri-modal with an increase of porosity and permeability according to the development of vugs and karsts.

RESULTS AND DISCUSSION

The electrical behaviour versus frequency for different porous solids textures is given in Figure 1. The complex impedance Z and phase angle θ decrease with a frequency ranging from 100 Hz to 100 kHz for any porous solids texture at full water saturation (Figure 1).

However, the gap between the maximum and minimum values of the complex impedance versus frequency is higher in « primary textures» than in « secondary textures ». This frequency dispersion is explained by the chargeability factor. The chargeability factor M depends strongly on the sedimentary rock texture (Table 1). The highest value of the chargeability factor *M* is observed in sedimentary M-W textures which range from 0.49 to 0.50. The sedimentary P-G textures show a medium chargeability factor

Table 1 : Electrical properties and water saturation determination of different studied samples.
F: formation factor; m : cementation factor; n : saturation exponent; Φw : water porosity; k_w : water permeability (mD);
ΦHg (%) : total mercury porosity; lc : characteritic length ;C : crystal carbonate; M-W- P: mudstone-wackestone-packstone.

Samples N°	Origin of porous materials	Texture	Φ_{Hg} (%)	l_c (nm)	**Electrical parameters** F	m	Chargeability	n	Φ_w (%)	k_w (mD)
1-C	Aquitain Danian dolomite	M-W	19.7	120094	35.56	2.05	0.388	2.9	17.5	27.43
2-C	"	M-W	26.6	35689	8.7	1.68	0.491	1.2	27.5	9.25
3-C	"	C	31	136888	20.6	2.48	0.366	1.87	31.1	203.225
4-C	"	C	29	95968	9.54	2.14	0.478	-	34.9	90.34
5-D	"	C	18.5	196256	23.28	1.98	0.411	2.6	20.4	142.9
6-D	"	C	21.5	249338	19.67	2.07	0.447	-	23.8	185.5
7-D	"	C	9.6	417695	13.77	1.99	0.423	2.4	26.8	303.4
8-D	"	M-W	16	5343	36.97	2.31	0.5	-	21.0	0.7
9-D	"	C	17	233725	28.2	2.27	0.483	3.4	22.9	169.96
1-sgrc5	Aquitain Stamp. limestone	P	26	258962	8.62	2.39	0.483	-	0.41	189.4
24-12B	"	P	41.3	203878	5.47	1.98	0.494	-	0.42	263.4
7-SC3	"	P	41.7	65282	13.17	2.47	0.446	3.28	0.35	41.3
23-12B	"	P	43	209252	5.18	1.94	0.502	1.9	0.43	491.1
10-SC2	"	M-W	32.4	278502	6.91	1.62	0.488	-	0.3	2047.2
9-SC2	"	M-W	20	31266	15.52	1.98	0.492	1.2	0.25	5

M ranging between 0.39 to 0.5. The lowest value of *M* is reached in the dolomitic crystal carbonate texture (with an intercrystalline pore-type, vuggy and karsts pore types) ranging from 0.37 to 0.48. The chargeability factor depends on the brine/gas saturation of porous solids. Figure 2B gives the relationship between the chargeability and brine saturation for two samples. We noted that *M* decreases significantly with the decrease of the brine saturation. The presence of vuggy and karsts pore types (sample 9-D) seems to speed up the decrease of *M*. So, when the brine is displaced by non-wetting and non-conducting fluid, the "chargeability" increases. The chargeability factor can be explained by a multi-linear model composed of different structure parameters such as water porosity and the Hg-fractal dimension of a porous medium. In the case of the shaly sandstone the chargeability factor increases with the salinity of brine in the porous medium.

In the F-Φ cross-plot, different experimental data sets satisfied the relationship $F \geq (3-\Phi)/2\Phi$ (Figure 1A). The cementation factor (m) and the structural parameters (a) were interpreted following two methods: i) The Archie method assumes a = 1, and *m* is determined for each sample from a logF-logΦ curve using equation (1) (Table 1, Figure 2A); ii) The best-fit method is applied for each textural class in order to obtain *a* and *m* (Figure 2A). The values of *m* obtained by using the first method, range from 1.62 to 2.48. The dolomitic cristal carbonate textures (textures III to IV) show the highest value of m (1.98 to 2.48) and F (9.54 to 36.97) while M-W and P textures have low values of m (1.62 to 1.98) and F (5.47 to 15.52). This high Archie cementation factor m of crystal carbonate is due to its high cementation degree. On the other hand, the best-fit electrical parameters were: *a* factor (ranged from 0.02 to 2.26) and *m* (ranged from 1.57 to 4.74) (Figure 2A). The comparison between different experimental data sets F-Φ and some predicted models allows us to conclude that the Archie's model (for carbonate rock) gives the best fit.

Figure 2E gives the relationship $\log I_R$ - $\log S_w$ and the saturation exponent *n* whose values range between 1.2 and 3.4. The highest value of *n* is obtained for crystal carbonate texture VI (n = 3.4) while the lowest value of *n* is obtained for mudstone-wackestone textures (n = 1.2). These parameters are not close to those given in literature (m = n = 2). These values are higher that those proposed by Archie's law and are usually used in petrophysics (n=2). A non-linear behaviour of the I_R-S_w curve is observed. The I_R-S_w plots change the slope at the saturation point where the corresponding capillary pressure curve indicates a transition from intergranular porosity to microporosity. High saturation exponents correspond to high values of the brine saturation and low saturation exponents correspond to low values of the brine saturation. The large pores have high saturation exponents (at low capillary pressures and low brine saturation), while small pores have low saturation exponents (at high capillary pressures and high brine saturation) due to the surface roughness and the water-wetting. These results are similar with some studies [17-

19]. Stalheim et al. [19] have pointed out that non-linear relationships can result a decreasing n with decreasing saturation (defined as a negative curvature). These negative curvatures depend on the formation properties: i) micro-porosity and rugged grain surface (give negative curvature), the salinity of the formation water; (ii) electrically conductive minerals; (iii) vugs or an electrically isolated pore space resulting in negative curvatures; (iv) fractures resulting in negative curvatures. Swanson [17] illustrated how microporosity in cherts and clays can also cause the saturation exponent to decrease as the water saturation decreases. Diederix [18] demonstrated how glass beads with a rough surface

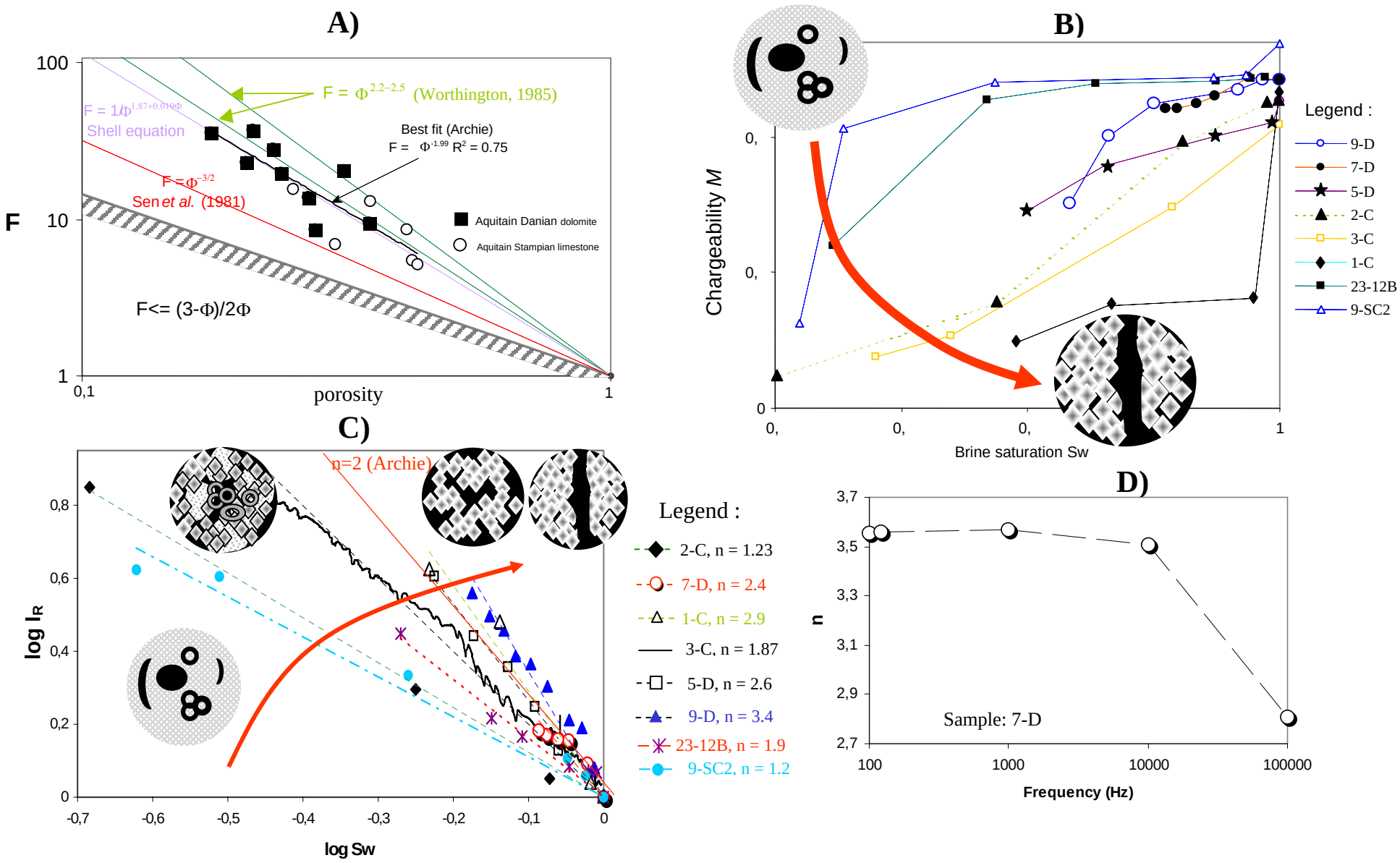

Figure 2. A) Formation factor (F) versus porosity (Φ) for different sedimentary textures; B) Chargeability *M* versus brine saturation for different sedimentary textures; C) Resistivity index versus brine saturation for different sedimentary textures; D) Saturation index variation versus frequencies.

texture exhibited a much lower saturation exponent than smooth-surface glass beads. The rough surface was responsible for retaining a relatively thick capillary water layer even at low water saturations. This influence is most pronounced in microporous rocks. The quality of water-gas saturation prediction depends on the quality of the electrical measurements. Indeed the desaturation technique using semi-permeable capillary diaphragms (ceramic membranes) was chosen to provide a homogeneous fluid distribution. On the other hand, measurements in a 4-electrod setting were chosen to avoid contact resistances, which can reach very high values (mainly when the water saturation decreases) and thus enhance the parameters drawn from a ratio R_t/Ro when rough values in 2-electrode settings are picked up. The saturation exponent values measured from 2-electrod and 4-electrod modes show a small gap. This can be explained by the low capillary end effects and a uniform saturation distribution along the core length. The saturation exponent n depends strongly on frequency (Figure 2D). So, when frequency increases from 100 Hz to 100 kHz the saturation exponent *n* decreases significantly from 3.56 to 2.181.

The comparison between the measured and predicted permeability from electrical parameters using different models is given in Figure 3. The best result is obtained with the Katz and Thompson model. In this model, the best-fit is obtained for a constant C on the order of 1/226. So, the characteristic length l_c of the pore space is the best adapted structural parameter in porous solids. Figure 3B gives a bilogarithmic version of the permeability prediction obtained from the Katz-Thompson model. The permeability is explained by the following relationship:

$$k_{KT} = \frac{l_c^{1.52}}{3.1 \cdot F^{0.64}} \tag{12}$$

Figure 3E shows a bilogarithmic crossplot of permeability k versus formation factor F for the selected samples following the Archie behaviour. The permeability is :

$$k = (28.05 / F^{1/6.25}) \tag{13}$$

The equation (13) shows a linear negative gradient between permeability and the formation factor. These results correspond to the Archie behaviour of a porous medium saturated by a high salinity, with a very low shaliness and a very large grain size.

CONCLUSIONS

The electrical behaviour in different frequencies of different sedimentary textures is investigated. The saturation exponent n depends strongly on the frequency and rock-textures and ranges between 1.2 and 3.4. A non-linear behaviour is observed. This is due to the high microporosity development and its roughness. The highest value of *n* is obtained for karstic dolomite textures. The frequency dispersion is explained by the chargeability factor *M*. The chargeability factor depends strongly on the sedimentary rock

texture. The highest value of the chargeability factor *M* is observed in sedimentary mudstone-wackestone textures while the lowest value is reached in the dolomitic crystal carbonate texture. We noted that *M* decreases hardly with the decrease of the brine saturation. The presence of vuggy and karsts pore types seems to speed up the decrease of *M*. Different models are investigated to obtain permeability from electrical parameters. The best result is obtained with the Katz and Thompson model.

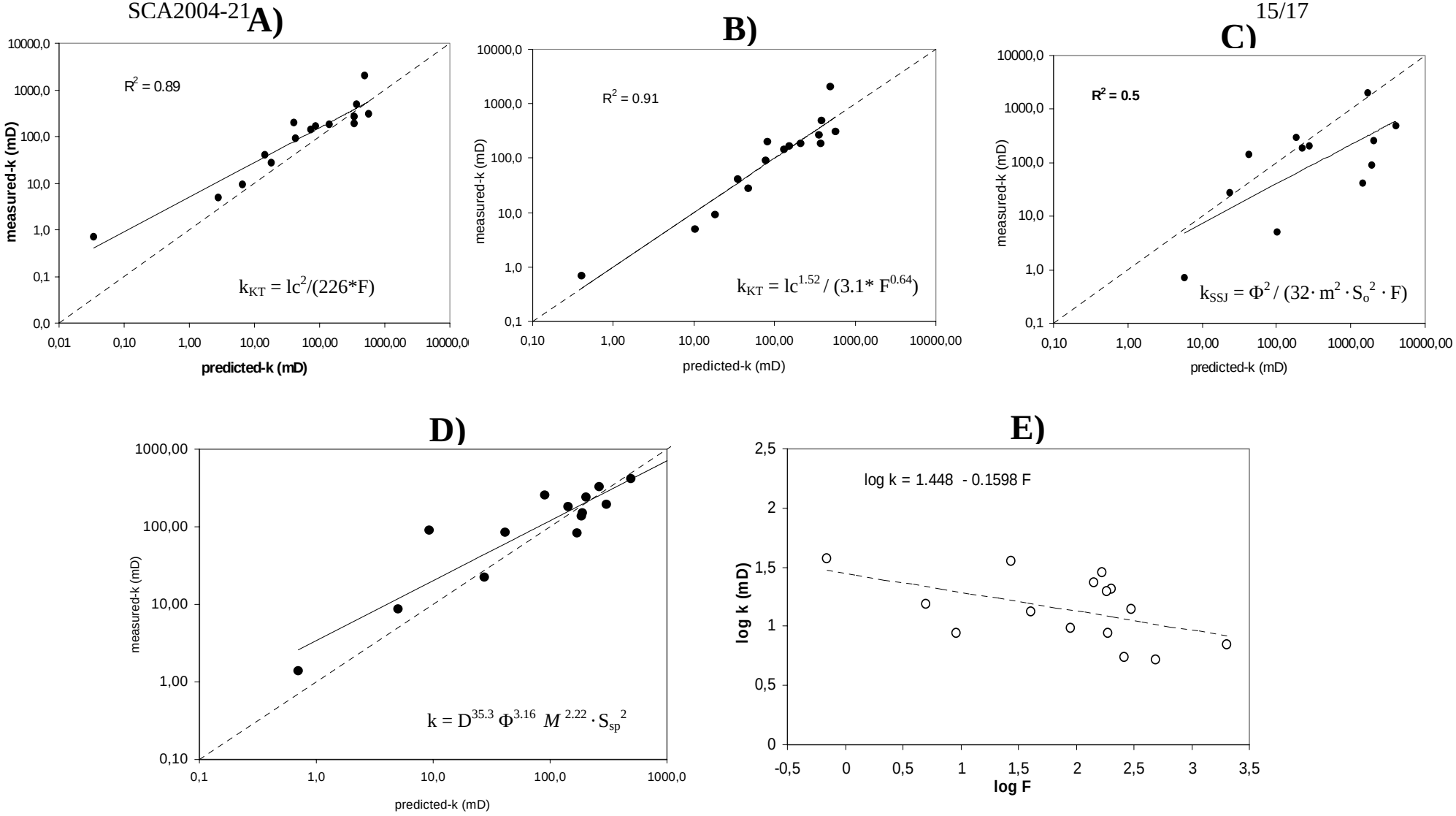

Figure 3. A) Permeability prediction from Katz-Thompson model, equation (8); B) Permeability prediction from a bilogarithmic version of Katz-Thompson model, equation (12); C) Permeability prediction from JPK model, equation (10); D) Permeability prediction from geometrical parameters such as: fractal dimension D, porosity Φ, chargeability *M* and surface area Ssp; E) Relationship between permeability k and formation factor F following the Archie behaviour.

REFERENCES

1. G.E. Archie, The electrical resistivity log as an aid in determining some reservoir characteristics, Trans. AIME 146 (1942) 54.
2. P.B. Basan, B.D. Lowden, P.R. Whattler, J.J. Attard, Pore-size data in petrophysics: a perspective on the measurement of pore geometry, Developments in Petrophysics, 122 (1997) 47-67.
3. H. Pape, C. Clauser and I. Joachim, Permeability prediction based on fractal pore-space geometry, Geophysics, 64 (1999) 1447-1460.
4. A. K. Moss, X.D. Jing and J.S. Archer, Wettability of reservoir rock and fluid systems from complex resistivity measurements, J. Pet. Sci. & Eng., 33 (2002) 75-85.
5. P.F. Worthington, Petrophysical estimation of permeability as a function of scale, from Lowell, M.A. & Hervey, P.K. (eds), in Developments in Petrophysics, Geological Society Special Publication, 122 (1997) 159-168.
6. B.R. Da Rocha and T.M. Habashy, Fractal geometry, porosity and complex resistivity: from rough pore interfaces to hand specimens, from Lowell, M.A. & Harvey, P.K., in Developments in Petrophysics, Geology Society Special Publication, 122 (1997) 277-286.
7. H.O. Seigel, Mathematical formulation and types curves for induced polarization, Geophysics 24 (1959) 547-563.
8. R. Wait, The variable-frequency method. In: Wait, J.R. (ed) Overvoltage Research and Geophysical Applications. Pergamon Press, New York (1959) 29-49.
9. A. Katz and A.H. Thompson, Fractal sandstone pores: Implications for conductivity and pore formation: Physical Review Letters 54 (1985) 1325-1329.
10. A. Katz and A.H. Thompson, Quantitative prediction of permeability in porous rock, Physical review B, 34 n° 11 (1986) 8179 – 8181.
11. A. Revil, P.A. Pezard and M. Darot, Electrical conductivity, spontaneous potential and ionic diffusion in porous media, in Developments in Petrophysics, Geology Society Special Publication, N° 122 (1997) 253-275.
12. L.M. Schwartz and P.N. Sen, Electrolyte conduction in partially saturated shaly formations. Annual Fall Technology Conference and Exhibition, Society of Petroleum Engineers, AIME, SPE paper 19131 (1988).
13. L.M. Schwartz, P.N. Sen and D.L. Johnson, Influence of rough surfaces on electrolytic conduction in porous media, Physical Review B40 (1989) 2540-2450.
14. D.L. Johnson and P.N. Sen, Dependence of the conductivity of a porous medium on electrolyte conductivity, Physical Reviews, B37 (1988) 3052-3510.
15. E.W. Washburn, Note on a method of determining the distribution of pore sizes in a porous material, Proc. Nat. Acad. Sci 7 (1921) 115-116.
16. S. Lowell and J .E. Shields, Powder surface area and porosity, Chapman and Hall, (1991) 46-140.
17. B.F., Swanson, Microporosity in reservoir rocks. Its measurement and influence on electrical resitivity. SPWLA 26th Annual Logging Symposium, june 17-20 1985.

18. K.M. Diederix, Anomalous relationship between resitivity index and water saturations in the Rotliegend sandstone (The netherlands), SPWLA 33th Annual Logging Symposium, july 6-9 1982.
19. S.O. Stalheim, T. Eidesmo, H. Rueslatten, Influence of wettability on water saturation modelling, J. Pet. Sci. Eng, 24 N°2-4 (1999) 243-253.